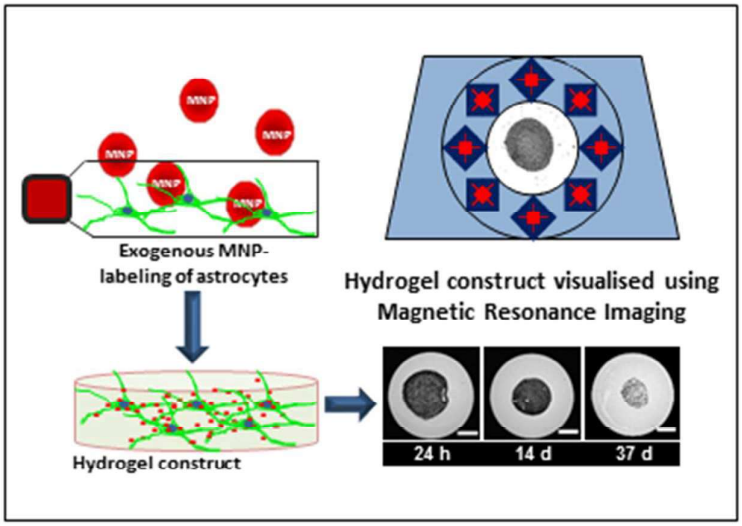

Graphical Abstract

Primary neural cells were exogenously-labeled with high magnetite content polymeric magnetic nanoparticles, prior to intra-construct incorporation within a 3-D collagen hydrogel. Combining the use of hydrogel technology with MRI compatible iron oxide nanoparticles has the potential to augment long-term survival of cell transplant populations, whilst offering the capacity for non-invasive MRI-tracking of intra-construct cells in neural cell therapy.

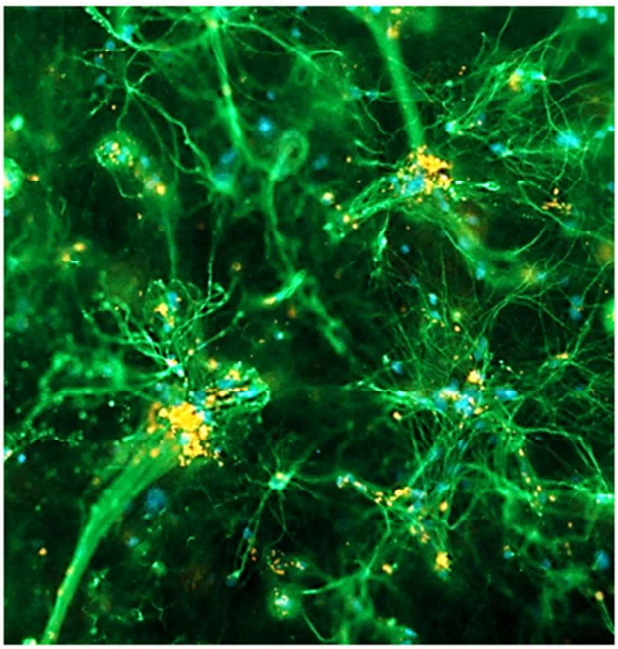

Cover figure (if required) –3-dimensional hydrogels facilitate a complex cellular network of MNP-labeled cortical astrocytes (21 d).

Executive summary

Delivery of transplant cells in protective and implantable materials can augment cell survival, enhancing efficacy of neural cell transplant delivery into the host parenchyma.

- Mouldable hydrogel-based materials capable of supporting 3-D cell growth offer key advantages as neuroprotective and immunomodulatory biomaterials.
- Methods to *non-invasively* track neural cell transplant populations in such matrices, using imaging methods are poorly developed.

Exogenous MNP labeled astrocytic hydrogels offer a promising approach as 3-dimensional implantable constructs.

- The macroporous nature of collagen hydrogels facilitated support of astrocyte growth in a viable and complex cellular network over an extended time frame. Morphological characterisation showed a significant difference in cell area, number and length ratio of primary processes across 14 d (***p <0.001) with cellular viability consistent at ca. 82%.
- MNP accumulation in astrocytes proved effective in providing a hypointense signal at 24h, 14d and 37d in astrocytic hydrogels.
- Proliferation was significantly higher at 24 h post-construct *vs*. 7d and 14 d in both non- and MNP-labeled cell hydrogels (*p <0.05). The influence of collagen on proliferation profiles of encapsulated astrocytes predicts low dilution of MNP-label with time, extending the utility of these particles as a contrast agent.

Hydrogel TEM facilitated study of astrocytic hydrogels.

- Astrocytic membrane was seen to be actively engaging with the collagen matrix.
- TEM confirmed the intracellular, peri-nuclear localisation of MNPs, seen as electron-dense areas with a hollow core; features consistent with their magnetite matrix.

Conclusion

- The construct developed offers the potential for *non-invasive* tracking of neural transplant populations delivered in encapsulating polymer matrices, over an extended time frame.

Abstract

Aim: (1) To develop a 3-dimensional neural cell construct for encapsulated delivery of transplant cells; (2) develop hydrogels seeded with magnetic nanoparticle (MNP)-labeled cells suitable for cell tracking by magnetic resonance imaging (MRI). **Materials/Methods:** Astrocytes were exogenously labeled with MRI-compatible iron-oxide MNPs prior to intra-construct incorporation within a 3-D collagen hydrogel. **Results:** A connective, complex cellular network was clearly observable within the 3-D constructs, with high cellular viability. MNP accumulation in astrocytes provided a hypointense MRI signal at 24h & 14 days. **Conclusions**: Our findings support the concept of developing a 3-D construct possessing the dual advantages of (i) support of long-term cell survival of neural populations with (ii) the potential for non-invasive MRI-tracking of intra-construct cells for neuroregenerative applications.

Keywords: astrocytes; 3-D collagen hydrogel; magnetic resonance imaging; transmission electron microscopy

Introduction

Cell transplantation is a major therapeutic approach for regenerative medicine following spinal cord injury (SCI). Results from early clinical transplantation trials demonstrate functional regeneration within the spinal cord, associated with some restoration of sensory and locomotor function [1, 2]. However, optimized neural cell transplantation depends on a number of factors, of which two are key. The first is achieving high viability and homogenous distribution following cell delivery into the host parenchyma. The second is the ability to non-invasively track the transplant cell population in host tissue over time such that the efficacy of cell therapy and bio-distribution can be monitored longitudinally.

The therapeutic efficacy of transplantation into the injury site is currently hampered by hurdles confronting the cell delivery process [3, 4]. One of the major confounding factors is the use of fine bore needles leading to clumping and shearing stress during delivery, causing extensive cell death [4-6]. Uneven settling and clumping can further lead to inhomogeneous cell distribution in lesion sites [3, 4], with variable repair. High levels of transplant cell death leads to macrophage infiltration, creating a further hostile microenvironment with additional cell loss [4]. These issues represent a critical translational barrier to neural cell therapy, highlighting the need to develop advanced cell delivery methodologies. It has been suggested that **the technical difficulties associated with surgical delivery of transplant cells can be attenuated by the use of a 3-dimensional protective cell matrix** provided by hydrogels [7-9]. These are highly hydrated networks of cross-linked polymers with their hydrophilic properties facilitating high water content [10]. Their protein composition directs self-assembly *in vitro* into a highly fibrous structure that resembles the mechano-elastic properties of the *in vivo* neural microenvironment [11]. These biomaterials are implantable and mouldable for ease of delivery to various lesion shapes [12, 13], and have limited effects on cell viability [10]. Hydrogels have been shown to promote neurological recovery and spinal

cord regeneration [14, 15] through incorporation of neurotrophic factors [16, 17, 18], offering structural support for ingrowing axons [19], and delivery of cell transplant populations for trophic support and recovery of a homeostatic environment [20, 21]. Cellular hydrogels offer a two-fold benefit for cell therapy, in that the neuroprotective and neuro-immunomodulatory mechanisms inherent to the incorporated cell population itself promote higher levels of cellular viability in the host tissue. In turn, this facilitates regeneration in spared axons, with the hydrogel construct acting as a bridge or scaffold across the lesion cavity [21].

Transplant cell tracking studies to date have shown a heavy reliance on carbocyanine dyes [10, 20, 22]; DNA identification of Y-chromosome probes [4]; retrograde tracing (e.g. using Fluorogold) [23]; radiolabelling or reporter protein expression [24, 25, 26]. Each has limitations in respect of imaging, toxicity and rapid decay of label [4, 27, 28] but the biggest obstacle is that the end point remains histological analysis, representing a major barrier to translational use. Therefore, there is a critical need to develop a non-invasive approach for the *in vivo* detection and tracking of cell transplant populations; widely shown to be achievable through the use of MNP-based contrast agents in conjunction with MRI; an imaging technique widely used in clinic. MNPs are a useful class of contrast agent as they result in a strong negative signal, enhancing cellular contrast, which addresses the low sensitivity associated with this imaging technique [29]. MRI of neural cell suspensions labeled with superparamagnetic MNPs has been extensively undertaken (i.e. OPCs [30]; NSCs [24]; ESCs [31, 32].

MRI of nanoparticle-labeled mesenchymal; bone-marrow and adipose-derived stem cells encapsulated within hydrogels has also been attempted [33, 34, 35]. A key point to note here is that the majority of neural transplantation studies, whether using dyes, genetic markers or MRI, *have used cells in suspension*; the non-invasive imaging methods have not been validated for neural cell - matrix constructs. Consequently, the concept of utilising MRI to

non-invasively track a neural cell transplant population **delivered within implantable matrices is a greatly under-investigated area in this emerging field of regenerative therapy.** Here we have attempted to develop a viable solution to these challenges using the transplant population of neonatal astrocytes (a major neural transplant population). These cells restore locomotor function when delivered as a cell suspension [25, 36, 37, 38, 39, 40, 41], but have been neglected as a transplant population delivered within a protective hydrogel environment. One study reported the transplantation of neonatal astrocytes encapsulated in collagen into the hemi-sected spinal cord [20]. Although partial restoration of locomotor function was reported, the utility of this cell: collagen construct was not developed further. Indeed, astrocyte characterisation within a 3-dimensional construct has only recently begun to be explored [10, 42, 43, 44, 45]. Notably, MNP-labeling of purified astrocytes results in extensive particle uptake with generation of high MRI contrast and no adverse effects on cell viability [46, 47]. Despite this, no study has investigated the feasibility of MNP-labeling of astrocytes to facilitate their non-invasive tracking within a protective matrix.

In light of these knowledge gaps, the goals of this study were to: 1) develop a 3-dimensional astrocyte construct with assessment of the safety of the protocols used, and 2) establish a MNP-labeled astrocytic hydrogel that can facilitate non-invasive MR imaging.

Materials & methods

The care and use of animals were in accordance with the Animals (Scientific Procedures) Act of 1986 (UK), and approved by the local ethics committee.

Astrocyte cell culture

Mixed glial cultures were established from disaggregated cerebral cortices of Sprague-Dawley rats (postnatal day 1-3), as described previously [47]. Briefly, following seven days

culture in D10 medium (Dulbecco's modified Eagle's medium, 2 mM glutaMAX-I, 1 mM sodium pyruvate, 50 U/ml penicillin, 50 µg/ml streptomycin and 10% fetal bovine serum), sequential overnight shakes facilitated astrocyte purification. Astrocytes were enzymatically detached using TrypLE™ (Life Technologies), and plated on poly-D-lysine coated T175 flasks and maintained in D10 medium for 24 h to allow for cell adherence.

High magnetite concentration MNPs as a contrast agent using MRI

The MNPs utilised for labeling of cortical astrocytes are as previously characterized [47, 48]. Briefly, the MNPs have a poly (lactic acid)/poly (vinyl alcohol) (PLA/PVA) coating, with a fluorescent BODIPY® 564/570-PLA coating and a high magnetite matrix loading [46.0 ± 1.08 (w/w)]; having a hydrodynamic diameter of 278 ± 1.62 nm and a negative charge (ζ-potential -14.4 ± 0.34 mV). These particles were a kind gift; prepared by the Boris Polyak Laboratory, Drexel University, Philadelphia, using published procedures [49]. Use of this MNP, due to its enhanced magnetite concentration, has been proven to be most effective in cellular uptake and long-term particle retention in cortical astrocytes as a monolayer culture [47]. Moreover, for the purposes of non-invasively tracking a MNP-labeled transplant population, a particle with such high magnetite concentration promises to generate a strong MR contrast.

Formation of collagen I hydrogel construct

Collagen I hydrogels (rat tail, high concentrate; Corning) were formulated to act as a 3-dimensional substrate for the protective delivery of neural cells as a cell transplant population. Collagen is a major protein and component of the extracellular matrix and has been utilised extensively as a 'functionalised scaffold' [14, 16, 17] and 3-dimensional cellular hydrogel [44, 45, 50]. Collagen hydrogels offer a biodegradable, homogenous, consistent composition of a porous, fibrillary network that provides structure to encapsulated cells [50,

51], allowing for ingrowth of neurites and facilitating guidance for axonal growth [52, 53]. The hydrogels were assembled using a published protocol [54]. Briefly, hydrogel composition was 80% collagen I (diluted in 0.6% acetic acid to 2 mg/mL); 10% Modified Eagle's Medium (MEM) Alpha (10x) and 10% cell suspension in D10 (1 x 10^6 cells/gel) with a final volume of 0.5 mL/gel, with NaOH (1M) used to obtain neutral pH. All components were kept on ice during hydrogel construct.

Development of a MNP-labeled cell: collagen I hydrogel construct

Exogenous labeling of cortical astrocytes with MNPs utilised a magnetofection protocol, as exposure to a magnetic field has shown enhanced levels of particle accumulation in these neural cells [47]. Briefly, lyophilised particles were added to D10 at a concentration of 26.5 µg/mL and added to astrocyte monolayers cultured in T175 flasks (15 mL/flask), followed by immediate exposure to a static magnetic field (F0) for 30 mins. Unlabeled cells (no particles) were also exposed to a magnetic field. At 24 h post-particle addition, cells were PBS rinsed (x2) to remove any free particles, enzymatically detached with TrypLE™; and the resulting MNP-labeled/unlabeled cell suspension added to collagen solution. Particle-labeled and unlabeled cell hydrogels were formed in a 24-well plate and allowed to set for 15 min at RT to allow for gradual increase in temperature from ca. 2° C prior to incubating for 1 h at 37° C (5% CO_2/95% humidified air). D10 medium was added over the top of the hydrogels (3 full medium changes over 90 mins to facilitate sufficient nutrient uptake). At 3 h post-construct, hydrogels were transferred to a larger 6-well plate to facilitate free floating of the gel in D10 (4 mL/well) (*Fig. 1 a & b)*, and maintained in D10 over the time course of the experiments, with a 50% medium change every 2-3 days. At specific assay time-points (24 h; 7 d; 14 d & 37 d), sample hydrogels were paraformaldehyde fixed (4% PFA; 3 h; RT). The cellular characteristics of the hydrogels were visualised using z-stack fluorescence microscopy (*Fig. 1*

c), with the utility of MNPs as a contrast agent for cell tracking visualised using MRI (*Fig. 1 d)*.

Preparing the hydrogels for MRI

To investigate the utility of the MNPs as a MRI contrast agent, PFA-fixed exogenous MNP-labeled cell hydrogels were prepared for MRI. Due to the small size of the gel, it was necessary to place them within a carrier tube (30 mL universal tube) for insertion into the MR scanner. The hydrogels were sandwiched between layers of agarose within the tube to prevent air pockets, which can generate imaging artefacts. A low-gelling temperature (<30° C) agarose gel (A4108 – Sigma, UK) was used to prevent damage to the hydrogels. Briefly, a 1% w/v agarose solution with PBS buffer was dissolved at melting point (>65° C), allowed to cool (~32° C), and 4 mL pipetted into the carrier tube and set at 4° C. The hydrogel was placed on this bottom layer before being sandwiched by a further layer of cooled agarose gel and stored upright at 4° C until imaging.

Preparing the hydrogels for Transmission Electron Microscopy (TEM)

To investigate subcellular features associated with particle uptake and trafficking, a novel technical modification was developed to facilitate visualisation of MNP-labeled cortical astrocytes within the hydrogel construct, utilising TEM. This entailed embedding the hydrogels within Spurr resin [55]. Briefly, following glutaraldehyde fix and initial steeping in osmium (2 h; RT), the hydrogels were rinsed in dH_2O (6x), placed in 70% ethanol (EtOH; 4h at RT), stored overnight in 80% EtOH (4° C) and taken through a modified series of EtOH dehydration steps before embedding in Spurr resin; modifying the standard protocol for use with collagen hydrogels. Following overnight storage in 80% EtOH, hydrogels were kept at 4 °C for a further period of 7 days during which time they were subject to an extended series of dehydration steps: 80% EtOH (24 h); 90 % EtOH (48 h - 100% refresh at 24 h); 100% EtOH

(48 h - 100% refresh at 24 h; 100% DRY EtOH (4 h - 100% refresh); 100% DRY EtOH (48 h). To embed in Spurr resin, hydrogels were infiltrated in 3:1 100% DRY EtOH:Spurr resin (24 h; RT), followed by 1:1 Spurr resin:100% DRY EtOH (4 h; RT); 3:1 resin:100% DRY EtOH (4 h; RT) before being infiltrated in pure Spurr resin overnight. The following day, hydrogels were infiltrated in fresh pure Spurr resin (8 h - 100% change every 2 h; RT) prior to embedding in fresh pure Spurr resin. Resin was polymerised for 24 h at 60° C. Ultrathin sections (100 nm) of the resin-embedded hydrogel were cut using a Reichert Ultracut E Microtome with the sections collected on 200-mesh thin bar grids. Intracellular particle uptake and trafficking were visualised from TEM micrographs taken from ultrathin sections using a JEOL-100CX TEM operating at an accelerating voltage of 100 kV.

Cellular viability assays

Cellular viability was quantified by cell counts, live/dead assays and EdU as a measure of proliferation. Cellular hydrogels (unlabeled and exogenous MNP-labeled) were subject to such assays at defined time points (24 h; 7 d; 14 d). For live/dead assays, hydrogels were incubated in a mixed solution of propidium iodide (5 µM), calcein (4 µM) and Hoechst 33342 (5 µg) in a final volume of 2 mL D10 medium per gel/well. Following 30 min incubation at 37° C (5% CO_2/95% humidified air), the hydrogels were PFA fixed, followed by PBS washes (x3) and fluorescence imaging for analysis. Click-iT® EdU (5-ethynyl-2´-deoxyuridine) cell proliferation assay was used as a measure of proliferative capacity of hydrogel-encapsulated astrocytes over time. Briefly, the protocol was as per manufacturer's instructions, with increases to volumes and incubation timings [56]. Specifically, 10 µM of EdU in a final volume of 1 mL D10 was added over the hydrogel followed by incubation at 37° C for 18 h. The hydrogels were then PFA fixed, followed by 4 washes with 3% bovine serum albumen (BSA). For permeabilisation, hydrogels were incubated in Triton-X 100 (0.5%) in PBS (40 min; RT). Permeabilisation was followed by 3% BSA wash (x4) prior to

the reagent cocktail being distributed over the hydrogel (1 mL/gel). The hydrogels were then incubated for 1 h at RT, protected from light, followed by 3% BSA wash (x2). Nuclei were counterstained with Hoechst 33342 (5 µg/mL PBS), and hydrogels incubated, protected from light (1 h; RT) prior to being washed in PBS (x4; 10 min/wash) to remove residual stain. Hydrogels were imaged immediately.

Morphological characterisation of cellular hydrogels

Morphological/morphometric features of unlabeled and MNP-labeled $GFAP^+$ cells in hydrogels were quantified – on a single cell basis - from z-stack fluorescence micrographs taken over 14 d post-construct. A measure of the ramified nature (branch-like processes) of $GFAP^+$ cells utilised the published formula: $\mathbf{4 \times \pi \times A/P^2}$ where **A**=*cell area* & **P**=*cell perimeter*. The calculated value of 1 denotes a rounded cell morphology, with values <1 indicative of a ramified morphology [56]. Average cell area and number of primary processes were quantified, with process length calculated as a length ratio based on the published formula: **L/D** where **L**=*process length (µm)* & **D**=*distance from nucleus to the tip of the process (µm)* [57].

Gel contraction

Formation of a cellular network causes gel contraction [11, 58]. To determine any adverse effect of gel contraction on cellular viability, culture characteristics were assessed across the time-frame of the experiment along with quantitative measures of the cell hydrogel across its diameter and depth (mm), obtained using z-stack fluorescence microscopy.

Immunocytochemistry

For protein detection and labeling of cellular architecture within the hydrogels, unlabeled and MNP-labeled cells were immunostained for glial fibrillary acidic protein (GFAP) with

fluorescein (FITC) secondary to enable assessment of cell count, morphological characteristics and intracellular localisation of particles. Protocols were based on published procedures for immunolabeling of hydrogels [54]. Briefly, following PFA fix and PBS washes, hydrogels were incubated in blocker (5% normal donkey serum and 0.5% Triton X-100 in PBS; 1 h; RT) followed by incubation in primary antibody, polyclonal rabbit anti-GFAP (Z0334; DakoCytomation, Ely, UK; 1:500 in blocker; 48 h at 4° C). Following PBS washes (x3; 15 min/wash) hydrogels were incubated in blocker (1 h; RT) prior to incubation in secondary antibody (FITC-labeled donkey anti-rabbit; 4 h; RT), protected from light. Hydrogels were washed in PBS (x3; 10 min/wash). To counterstain for nuclei, Hoechst 33342 was added (5 µg/mL PBS) and hydrogels incubated, protected from light (1 h; RT). To remove residual stain, hydrogels were PBS washed (x4; 10 min/wash) before being imaged.

Z-stack fluorescence imaging

Hydrogels were transferred into a CELLview™ glass-bottom petri dish for imaging. Quantification and subsequent analysis of culture characteristics, experimental outcomes and cellular viability assessments were assessed from triple-merged (RGB fluorescence) z-stack images (*Fig. 1 c)*, acquired from four random fields at the centre and edges of the gel with comparative counts taken from the base, middle and top layer of the hydrogel. These were captured at 100-200x magnification using a Zeiss Axio Observer.Z1 microscope fitted with a Zeiss AxioCam MR R3 digital camera and a *p*E-300 CoolLED fluorescence unit and utilising the Blue Edition ZEN 2 software, version 2.0.

MR Imaging

The utility of MNPs as a suitable contrast agent for tracking a neural cell population was assessed via MRI. MR imaging of the hydrogel constructs was conducted using a Bruker 9.4 T Avance III HD instrument (Bruker, Coventry, UK) utilising a 40 mm transmit/receive

quadrature volume coil. High resolution three-dimensional T_2^* weighted images were acquired with a FLASH sequence with the following parameters: field of view 25x25x4 mm, matrix size 256x256x40, echo time (TE) 8 ms, repetition time (TR) 400 ms, averages 2, flip angle 20°, scan time 2h 37min.

Dynamic time-lapse imaging

Particle inheritance in daughter cells of MNP-labeled dividing astrocytes within hydrogel constructs was assessed from dynamic time-lapse images captured at a frequency of 1 frame/180 s over a period of at least 48 h. Images were captured from the transmitted light (97 ms exposure) and BODIPY® 564/570 (500 ms exposure) fluorescence channels using an Axio Zoom V16 microscope fitted with an AxioCam ICm1 camera and utilising Blue Edition ZEN software, version 1.1.1.0.

Statistical analyses

Experimental data were analysed by one-way analysis of variance (ANOVA) with *post-hoc* analysis carried out using Bonferroni's multiple comparison test (MCT). All data are expressed as mean ± standard error of the mean (s.e.m) with *'n'* referring to the number of different experiments within each particular study, each derived from a different rat litter. Analysis was conducted using Prism statistical analysis software, version 7 (GraphPad Software Inc.).

Results

Astrocyte characteristics and viability within a 3-dimensional construct

At 24 h post-construct production, the majority of cells retained rounded morphologies typically observed following enzymatic detachment, with a few cells beginning to elaborate processes (*Fig. 2 a)*. At 7 d, the majority of cells were processed within the construct, with an

emergent cell network evident (*Fig. 2 b)*. A highly connective, complex cellular network was clearly observable at 14 d post-construct, with large networks of aligned "bundles" of astrocytic processes present throughout the hydrogel. Astrocytes showed a small cell soma and stellate morphology (*Fig. 2 c)*. Cell clumping within the hydrogel was negligible (ca. <1% - data not shown). For the cellular hydrogels developed here, the average cell counts per unit area remained constant, although a significant decrease was noted following the initial time-point (*Fig. 2 d)*. Cellular viability remained consistently high throughout the time period studied (*ca.* 82%); decreasing from 82 % at 24 h to 78 % at 7 d, before showing an increase to 85% at 14 d (*Fig. 2 e)*. The cellular hydrogels in this study showed significant contraction with reduction in diameter over 14 d [***$p < 0.001$ (*Fig. 2 f & g)*], but not depth (data not shown). Morphological measurements of cells grown within constructs showed no difference between unlabeled and MNP-labeled cellular hydrogels (*Fig. 3*). Cortical astrocytes took on a highly ramified nature over time (*Fig. 3 a*) with a significant increase seen in cell area (*Fig. 3 b*), number of- and average length ratio of- primary processes over 14 days post-construct (*Fig. 3 c & d, respectively*) (***p <0.001).

TEM to visualise intracellular MNP accumulation

At 24 h post-construct, high intracellular particle accumulation was noted in astrocytes (*Fig. 4 a & b; b; arrows*). It should be noted that exogenously labeled cells in monolayer culture (*Fig. 4 a)* possessed distinct morphologies to those observed for cells encapsulated within the hydrogel (*Fig. 4 b)*. As with unlabeled cell hydrogels, a highly connective, cellular network was evident with a high level of intracellular particle retention and peri-nuclear particle localisation still evident at 14 d (*Fig. 4 c)*. TEM facilitated study of astrocytic hydrogels. Cell membranes were seen to be actively engaging with the collagen substrate (*Fig. 4 d; arrow heads)*. MNPs could be seen as electron dense areas, with a hollow core surrounded by a dense 'ring'; features consistent with the magnetite matrix composition of these particles

(*Fig. 4 d; arrows)*. TEM confirmed the intracellular, peri-nuclear localisation of MNPs at 15 d (*Fig. 4 d)*.

Cellular viability of MNP-labeled astrocytic hydrogel

Cellular viability assays showed no significant difference over time between unlabeled and MNP-labeled cell hydrogels (*Fig. 2 d & e vs. Fig. 4 e & f)*. Quantification of cell number revealed a similar pattern for both unlabeled and MNP-labeled cell hydrogels, although the decrease in cell count noted after 24 h was not significant in MNP-labeled cells *(Fig. 4 e)*. Cellular viability remained consistent at *ca.* 82% across the time-frame (*Fig. 4 f)*.

Utility of high magnetite concentration MNPs as a contrast agent

In respect of their utility as a contrast agent for MRI within the MNP-labeled cell hydrogels, the levels of MNP accumulation in astrocytes proved effective in providing a hypointense signal at 24 h and 14 d (*Fig. 4 g - j)*. Across the time-frame, a clear distinction could be made between the hypointense signal recorded from MNP-labeled cell hydrogels versus that of unlabeled astrocytic hydrogels (*compare Fig. 4 g & i vs. h & j)*.

Proliferation profile of encapsulated astrocytes

Dividing astrocytes were clearly observed within the hydrogels (*Fig. 5 a)*. Proliferation was significantly higher at the initial time-point but remained consistently low thereafter, indicating a relatively quiescent population (*Fig. 5 b)*. Use of dynamic time-lapse imaging enabled visualisation of cell division in real time within these hydrogels (*Fig. 5 c – h; see Supplementary Video*), with particles inherited by the daughter cells (*Fig. 5 h; arrows)*.

Utility of MNPs for non-invasive cell tracking over extended time period

At the later time point of 37 d, a clear distinction in contrast between unlabeled and MNP-labeled cell hydrogels could still be detected (*Fig. 6 a; MNP-labeled vs. b; unlabeled)*, although less than that recorded at earlier time points (*Fig. 6 a vs. Fig. 4 g & i)*. Hypointense

'spots' were observed throughout the gel (*Fig. 6 a)* suggesting either localised particle clumping within the gel *or* particle retention within localised foci of cells. The latter possibility was corroborated by confocal fluorescence microscopy (*Fig. 6 c)* offering clear evidence of intracellular particle retention, and peri-nuclear localisation of particles at this extended time-point (*Fig. 6 c; arrows*). Microscopic observations at 37 d (*Fig. 6 d*) were indicative of high cellular viability.

Discussion

Protective neural cell delivery systems offer a viable solution to the technical issues faced during transplantation for neuroregenerative therapy. It is now widely accepted that cells removed from their *in vivo* environment display atypical morphologies when cultured on 2-dimensional 'hard' substrates [57]. Accordingly, development of 3-dimensional constructs is a rapidly emergent field for therapeutic cell transplantation. We report a robust protocol to generate a protective delivery system for MNP-labeled astrocytes, with potential for imaging of intra-construct cells. We believe the fusion of the astrocyte- MNP- hydrogel elements offers an advanced therapeutic approach in the form of (1) a 3-dimensional, protective hydrogel matrix, containing (2) an MNP-labeled astrocyte population which (3) has the potential to be tracked non-invasively using MRI.

Several technical considerations needed to be accounted for in facilitating the development of a viable 3-dimensional neural cell construct. The novel technical development of embedding the hydrogels within a resin carrier allowed effective use of TEM to study morphologies, membrane features and intracellular particle localisation in these soft matrices. Within these hydrogels, a high level of membrane interaction with the collagen matrix was evident. From this it could be speculated that this mechanism is related to remodelling and (re)adapting of the environment by cells [11, 58]. Astrocytes in the free-floating gels in this study showed a

small cell soma and stellate morphology with a complex, connective network of threadlike processes, as reported previously [42]. This in contrast to cortical astrocytes grown within anchored gels, which have been reported to be predominantly bipolar in shape and aligned to the tension exerted upon the gel [59, 60]. Further, astrocytes grown on hard substrates such as glass or culture plastics exhibit two distinct phenotypes: a type 1 flat, membranous unbranched morphology, and a type 2 with small soma and highly branched, more complex morphology. This extensive variability in astrocyte phenotype highlights the profound influence of substrate mechano-elastic properties on cellular behaviours. We consider this new ultrastructural imaging approach for soft polymer materials to be of key importance in understanding cell characteristics within a 3-dimensional matrix environment.

A major challenge in clinical cell therapy is lowered regenerative efficacy due to the presence/delivery of dead and dying transplant cells [3-5]. Consequently, the safety of our protocols was of paramount concern. Due to its macroporous nature, cellular remodelling of the collagen fibrillar matrix contracts the hydrogel, with the extent of contraction directly related to both cell density and polymer concentration. Rapid contraction occurs within 12 h but contraction rates decrease thereafter [61]; a phenomenon observed in the astrocytic hydrogels in this study. However, in line with other reports, the high cellular viability observed in these hydrogels suggests that gel contraction had no adverse effects on cell survival [10]. A drop in average cell number following 24 h post-construct was noted within the hydrogels, although cellular viability remained consistent over the time period studied. In turn, a higher proliferation rate was reported at 24 h which decreased significantly thereafter. This, combined with the low level of cell death occurring over the time-frame, may account for the initial drop in cell number *and* the consistent cellular viability observed within the hydrogels. Indeed, cellular viability over an extended time-frame suggests effective

availability of oxygen and nutrients to, and efficient removal of metabolic waste products from, the cellular hydrogels [62, 63].

MNPs previously validated for astrocyte labeling were utilised in these gels due to the high level of uptake, accumulation and long-term retention [47]. The growth of the cell populations is of critical importance for cell tracking, as high proliferative capacity - a feature previously observed in both unlabeled and MNP-labeled astrocyte monolayer cultures [47] - results in label dilution [64, 65]. Within all hydrogels, proliferation overall remained consistently low across the time period studied indicating a relatively quiescent population. Two factors may account for this. Extracellular matrix proteins within collagen I are known to regulate the proliferative capacity of cells [11], and gel contraction can downregulate extracellular signal regulated kinase which arrests cells in G_0 phase of the cell cycle [60]. These alterations are relevant as studies report that only 35% of cell-cycle-arrested astrocytes, return to the cell cycle [66]. This low proliferative capacity would predict low dilution of MNP-label, thereby extending the utility of these particles as a contrast agent for non-invasive cell tracking using MRI. This requires confirmation in *in vivo* studies.

TEM showed clear evidence of intracellular particle accumulation and peri-nuclear localisation- a prominent feature in these astrocytic hydrogels. This particle accumulation proved highly efficient in providing a hypointense signal at 24 h through 14 d to 37 d post-construct. Regarding the fate of MNPs in the gel, exocytosis may play a role in particle release, with either vesicle or lysosome secretion factoring in particle trafficking from the cell [67]; although, the observed decrease in levels of free particles from 48 h onwards suggests continued cellular particle uptake from within the gel. Cell division results in particle dilution with subsequent inheritance of the particles by daughter cells [64, 65]; particle loss may occur during cell division. However, in these hydrogels proliferative capacity was significantly reduced from day 7 onwards, suggesting a higher level of particle retention over

time. A reasonable proposition therefore, for the lowered hypointensity observed at 37 d and one which we cannot rule out, is the possibility of 'washout' of extracellular MNPs from the gel into the media, which, given the macroporous nature of the collagen gel may be a possibility. Even so, while lower hypointensity overall was recorded at this extended time-point, hypointense 'spots' were observed suggesting localised particle retention in cells. This possibility was corroborated by fluorescence microscopy, thus verifying the construct's continued utility over an extended time frame.

The 'proof of concept' presented here substantiates the notion that the developed construct offers the potential for tracking of neural transplant populations, delivered in encapsulating polymer matrices, over an extended time frame. Future work will extend the findings from this study to a range of neural transplant populations with the testing of cell tracking capacity in live animal models of neurological injury, such as spinal cord transection models. Such studies will need to take account of hydrogel breakdown properties in host neural tissue, along with the unique proliferative and differentiation behaviours of individual transplant populations and their labeling capacity using nanoparticle platforms.

References.

Papers of special note have been highlighted as:

* of interest; * of considerable interest

Electronic Supplementary Material: Supplementary material showing a MNP-labeled cortical astrocyte undergoing division at 7 d post-hydrogel-construct is available in the online version of this article at http://dx.doi.org/10.1007/*****

[1] Granger N, Blamires H, Franklin RJ, Jeffery ND. Autologous olfactory mucosal cell transplants in clinical spinal cord injury: a randomized double-blinded trial in a canine translational model. *Brain.* 135**,** 3227-37 **(**2012).

[2] Tabakow P, Raisman G, Fortuna W *et al*. Functional regeneration of supraspinal connections in a patient with transected spinal cord following transplantation of bulbar olfactory ensheathing cells with peripheral nerve bridging. *Cell Transplant.* 23, 1631-55 (2014).

[3] Guest J, Benavides F, Padgett K, Mendez E, Tovar D. Technical aspects of spinal cord injections for cell transplantation. Clinical and translational considerations. *Brain Res Bull.* 84**,** 267-79 (2011)

****Examines the issues inherent to surgical delivery of cell transplant populations; see also [5] Amer et al (2015)**

[4] Pearse DD, Sanchez AR, Pereira FC *et al*. Transplantation of Schwann cells and/or olfactory ensheathing glia into the contused spinal cord: Survival, migration, axon association, and functional recovery. *Glia.* 55, 976-1000 (2007).

[5] Amer MH, White LJ, Shakesheff KM. The effect of injection using narrow-bore

needles on mammalian cells: administration and formulation considerations for cell therapies. *J Pharm Pharmacol.* 67(5), 640-650 (2015).

[6] Hill CE, Hurtado A, Blits B *et al*. Early necrosis and apoptosis of Schwann cells transplanted into the injured rat spinal cord. *Eur J Neurosci.* 26, 1433-45 (2007).

[7] Siebert JR, Eade AM, Osterhout DJ. Biomaterial approaches to enhancing neurorestoration after spinal cord injury: Strategies for overcoming inherent biological obstacles. *Biomed Res Int*. 752572 (2015).

[8] Vater C, Lode A, Bernhardt A, Reinstorf, A, Heinemann C, Gelinsky M. Influence of different modifications of a calcium phosphate bone cement on adhesion, proliferation, and osteogenic differentiation of human bone marrow stromal cells. *J Biomed Mater Res A.* 92, 1452-60 (2010).

[9] Perale G, Rossi F, Sundstrom E, *et al*. Hydrogels in spinal cord injury repair strategies. *ACS Chem Neurosci.* 2, 336-45 (2011).

**** Review of 3-D construct's utility for cell transplantation**

[10] Frampton JP, Hynd MR, Shuler ML, Shain W. Fabrication and optimization of alginate hydrogel constructs for use in 3D neural cell culture. *Biomed Mater.* 6, 015002 (2011).

[11] Trappmann B, Chen CS. How cells sense extracellular matrix stiffness: a material's perspective. *Curr Opin Biotechnol.* 24, 948-53 (2013).

[12] Hejcl A, Lesny P, Pradny M *et al*. Biocompatible hydrogels in spinal cord injury repair. *Physiological Research.* 57, S121-S132 (2008).

[13] Perale G, Bianco F, Giordano C, Matteoli M, Masi M, Cigada A. Engineering

injured spinal cord with bone marrow derived stem cells and hydrogel based matrices: a glance at the state of art. *J Appl Biomater Biomech.* 6, 1-8 (2008).

[14] Kaneko A, Matsushita A, Sankai YA. 3D nanofibrous hydrogel and collagen sponge scaffold promotes locomotor functional recovery, spinal repair, and neuronal regeneration after complete transection of the spinal cord in adult rats. *Biomed Mater.* 10, 015008 (2015).

[15] Li K, Javed E, Hala TJ, *et al*. Transplantation of glial progenitors that overexpress glutamate transporter GLT1 preserves diaphragm function following cervical SCI. *Mol Ther.* 23, 533-48 (2015).

[16] Han Q, Jin W, Xiao Z, *et al*. The promotion of neural regeneration in an extreme rat spinal cord injury model using a collagen scaffold containing a collagen binding neuroprotective protein and an EGFR neutralizing antibody. *Biomaterials.* 31, 9212-20 (2010).

[17] Geral C, Angelova A, Lesieur S. From molecular to nanotechnology strategies for delivery of neurotrophins: Emphasis on brain-derived neurotrophic factor (BDNF). *Pharmaceutics*. 5, 127-167 (2013).

[18] Liang W, Han Q, Jin W, *et al*. The promotion of neurological recovery in the rat spinal cord crushed injury model by collagen-binding BDNF. *Biomaterials.* 31, 8634-41 (2010).

[19] Li K, Javed E, Scura D, *et al*. Human iPS cell-derived astrocyte transplants preserve respiratory function after spinal cord injury. *Exp Neurol.* 271, 479-92 (2015).

[20] Joosten EA, Veldhuis WB, Hamers FP. Collagen containing neonatal astrocytes stimulates regrowth of injured fibers and promotes modest locomotor recovery after spinal cord injury. *J Neurosci Res.* 77, 127-42 (2004).

[21] De Paul MA, Palmer M, Lang BT, *et al*. Intravenous multipotent adult progenitor cell treatment decreases inflammation leading to functional recovery following spinal cord injury. *Sci Reports.* 5, 16795, DOI: 10.1038/srep16795 (2015).

**** Demonstrates utility of 3-D cellular construct for regenerative therapy**

[22] O'Shaughnessy TJ, Lin HJ, Ma W. Functional synapse formation among rat cortical neurons grown on three-dimensional collagen gels. *Neuroscience Letters.* 340**,** 169-172 (2003).

[23] Kushchayev SV, Giers MB, Hom Eng D, *et al*. Hyaluronic acid scaffold has a neuroprotective effect in hemisection spinal cord injury. *J Neurosurg Spine.* 25**,** 114-24 (2016).

[24] Bulte JW, Douglas T, Witwer B, *et al*. Magnetodendrimers allow endosomal magnetic labeling and in vivo tracking of stem cells. *Nat Biotechnol.* 19**,** 1141-7 (2001).

[25] Filous AR, Miller JH, Coulson-Thomas YM, Horn KP, Alilain WJ, Silver J. Immature astrocytes promote CNS axonal regeneration when combined with chondroitinase ABC. *Dev Neurobiol.* 70**,** 826-41 (2010).

[26] Kircher MF, Gambhir SS, Grimm J. Noninvasive cell-tracking methods. *Nat Rev Clin Oncol.* 8**,** 677-88 (2011).

[27] Hossain MA, Frampton AE, Bagul A. Challenges facing in vivo tracking of mesenchymal stem cells used for tissue regeneration. *Expert Rev Med Devices.* 11**,** 9-13 (2014).

[28] Mertens ME, Frese J, Bolukbas DA, *et al*. FMN-coated fluorescent USPIO for cell labeling and non-invasive MR imaging in tissue engineering. *Theranostics.* 4**,** 1002-13 (2014).

[29] Bulte JW, Kraitchman DL. Iron oxide MR contrast agents for molecular and cellular imaging. *NMR Biomed.* 17**,** 484-99 (2004).

[30] Bulte JW, Zhang S, Van Gelderen P. Neurotransplantation of magnetically labeled oligodendrocyte progenitors: magnetic resonance tracking of cell migration and myelination. *Proc Natl Acad Sci U S A.* 96**,** 15256-61 (1999).

[31] Hoehn M, Kustermann E, Blunk J, *et al*. Monitoring of implanted stem cell migration in vivo: a highly resolved in vivo magnetic resonance imaging investigation of experimental stroke in rat. *Proc Natl Acad Sci U S A.* 99**,** 16267-72 (2002)

[32] Jendelova P, Herynek V, Urdzikova L, *et al.* Magnetic resonance tracking of transplanted bone marrow and embryonic stem cells labeled by iron oxide nanoparticles in rat brain and spinal cord. *J Neurosci Res.* 76**,** 232-43 (2004).

[33] Cen L, Neoh KG, Sun J, *et al.* Labeling of adipose-derived stem cells by oleic-acid-modified magnetic nanoparticles. *Advanced Functional Materials.* 19**,** 1158-1166 (2009).

[34] Heymer A, Haddad D, Weber M, *et al.* Iron oxide labelling of human mesenchymal stem cells in collagen hydrogels for articular cartilage repair. *Biomaterials.* 29**,** 1473-83 (2008).

[35] Sykova E, Jendelova P, Urdzikova L, Lesny P, Hejcl A. Bone marrow stem cells and polymer hydrogels--two strategies for spinal cord injury repair. *Cell Mol Neurobiol.* 26**,** 1113-29 (2006).

[36] Davies JE, Huang C, Proschel C, Noble M, Mayer-Proschel M, Davies SJ. Astrocytes derived from glial-restricted precursors promote spinal cord repair. *J Biol.* 5**,** 7 (2006).

[37] Davies SJ, Shih CH, Noble M, Mayer-Proschel M, Davies JE, Proschel C. Transplantation of specific human astrocytes promotes functional recovery after spinal cord injury. *PLoS One.* 6**,** e17328 (2011).

**** Demonstrates utility of astrocytes as neural transplant population**

[38] Fan C, Zheng Y, Cheng X, *et al*. Transplantation of D15A-expressing glial-restricted-precursor-derived astrocytes improves anatomical and locomotor recovery after spinal cord injury. *Int J Biol Sci.* 9**,** 78-93 (2013).

[39] Pencalet P, Serguera C, Corti O, Privat A, Mallet J, Gimenez Y, Ribotta M. Integration of genetically modified adult astrocytes into the lesioned rat spinal cord. *J Neurosci Res*. 83**,** 61-7 (2006).

[40] Selkirk SM, Greenberg SJ, Plunkett RJ, Barone TA, Lis A, Spence PO. Syngeneic central nervous system transplantation of genetically transduced mature, adult astrocytes. *Gene Ther.* 9**,** 432-43 (2002).

[41] Wang JJ, Chuah MI, Yew DT, Leung PC, Tsang DS. Effects of astrocyte implantation into the hemisected adult rat spinal cord. *Neuroscience.* 65**,** 973-81 (1995).

[42] Balasubramanian S, Packard JA, Leach JB, Powell EM. Three-dimensional environment sustains morphological heterogeneity and promotes phenotypic progression during astrocyte development. *Tissue Eng Part A.* 22**,** 885-98 (2016).

**** Examines influence of 3-D construct on astrocyte characterisation**

[43] Placone AL, Mcguiggan PM, Bergles DE, Guerrero-Cazares H, Quinones-Hinojosa A, Searson PC. Human astrocytes develop physiological morphology and remain quiescent in a novel 3D matrix. *Biomaterials*. 42**,** 134-43 (2015).

[44] Seyedhassantehrani N, Li Y, Yao L. Dynamic behaviours of astrocytes in chemically modified fibrin and collagen hydrogels. *Integr Biol (Camb).* 8**,** 624-34 (2016).

[45] Winter CC, Katiyar KS, Hernandez NS, *et al*. Transplantable living scaffolds comprised of micro-tissue engineered aligned astrocyte networks to facilitate central nervous system regeneration. *Acta Biomater.* 38**,** 44-58 (2016).

[46] Pickard MR, Jenkins SI, Koller CJ, Furness DN, Chari DM. Magnetic nanoparticle labeling of astrocytes derived for neural transplantation. *Tissue Eng Part C Methods.* 17**,** 89-99 (2011).

*** Examines utility of MNP-labeling as contrast agent**

[47] Tickle JA, Jenkins SI, Polyak B, Pickard MR, Chari DM. Endocytotic potential governs magnetic particle loading in dividing neural cells: studying modes of particle inheritance. *Nanomedicine (Lond).* 11**,** 345-58 (2016).

[48] Adams CF, Rai A, Sneddon G, Yiu HH, Polyak B, Chari DM. Increasing magnetite contents of polymeric magnetic particles dramatically improves labeling of neural stem cell transplant populations. *Nanomedicine.* 11**,** 19-29 (2015).

[49] Johnson B, Toland B, Chokshi R, Mochalin V, Koutzaki S, Polyak B. Magnetically responsive paclitaxel-loaded biodegradable nanoparticles for treatment of vascular disease: preparation, characterization and in vitro evaluation of anti-proliferative potential. *Curr Drug Deliv.* 7**,** 263-73 (2010).

[50] Hawkins BT, Grego S, Sellgren KL. Three-dimensional culture conditions differentially affect astrocyte modulation of brain endothelial barrier function in response to transforming growth factor beta1. *Brain Res.* 1608, 167-176 (2015).

[51] Macaya D, Spector M. Injectable hydrogel materials for spinal cord regeneration: a review. *Biomed Mater.* 7, 012001 (2012).

[52] Willits RK, Skornia S. Effect of collagen gel stiffness on neurite extension. *J Biomater Sci Polym Ed.* 15, 1521-1531 (2004).

[53] Katiyar KS, Winter CC, Struzyna LA, Harris JP, Cullen DK. Mechanical elongation of astrocyte processes to create living scaffolds for nervous system regeneration. *J Tissue Eng Regen Med.* 11, 10, 2737-2751 (2017).

[54] Phillips JB, Brown RA. Micro-structured materials and mechanical cues in 3D collagen gels. In: *3D Cell Culture: Methods and Protocols, Methods in Molecular Biology (Volume 12)*, Haycock JW (Ed.), Springer Science+Business Media LLC, London, UK, 183-196 (2011).

[55] Spurr AR. A low-viscosity epoxy resin embedding medium for electron microscopy. *J Ultrastruct Res.* 26**,** 31-43 (1969).

[56] East E, Golding JP, Phillips JB. A versatile 3D culture model facilitates monitoring of astrocytes undergoing reactive gliosis. *J Tissue Eng Regen Med.* 3**,** 634-46 (2009).

[57] Hu WW, Wang Z, Zhang SS *et al.* Morphology and functions of astrocytes cultured on water-repellent fractal tripalmitin surfaces. *Biomaterials.* 35, 7386-7397 (2014).

[58] Wakatsuki T, Elson EL. Reciprocal interactions between cells and extracellular matrix during remodeling of tissue constructs. *Biophys Chem.* 100**,** 593-605 (2003).

[59] East E, De Oliveira DB, Golding JP, Phillips JB. Alignment of astrocytes increases neuronal growth in three-dimensional collagen gels and is maintained following plastic compression to form a spinal cord repair conduit. *Tissue Eng Part A.* 16**,** 3173-84 (2010).

[60] Grinnell F. Fibroblast-collagen-matrix contraction: growth-factor signalling and mechanical loading. *Trends Cell Biol.* 10**,** 362-5 (2000).

[61] Brown RA. In the beginning there were soft collagen-cell gels: towards better 3D connective tissue models? *Exp Cell Res.* 319**,** 2460-9 (2013).

[62] Malda J, Woodfield TB, Van Der Vloodt F *et al.* The effect of PEGT/PBT scaffold architecture on oxygen gradients in tissue engineered cartilaginous constructs. *Biomaterials.* 25, 5773-57780 (2004).

[63] Mertens ME, Hermann A, Buhren A *et al.* Iron oxide-labeled collagen scaffolds for non-invasive MR imaging in tissue engineering. *Adv Funct Mater.* 24, 754-762 (2014).

[64] Harrison R, Markides H, Morris RH, Richards P, El Haj AJ, Sottile V. Autonomous magnetic labelling of functional mesenchymal stem cells for improved traceability and spatial control in cell therapy applications. *J Tissue Eng Regen Med.* **DOI**: 10.1002/term.2133 (2016).

[65] Kim JA, Aberg C, Salvati A, Dawson KA. Role of cell cycle on the cellular uptake and dilution of nanoparticles in a cell population. *Nat Nanotechnol.* 7**,** 62-8 (2012).

[66] Murphy S. Generation of astrocyte cultures from normal and neoplastic central nervous system. In: *Methods in Neurosciences: Cell Culture (Volume 3).* Conn PM (Ed.), Academic Press Inc, 33-47 (1990).

[67] Oh N, Park JH. Endocytosis and exocytosis of nanoparticles in mammalian cells. *Int J*

Nanomedicine. 9, Suppl 1, 51-53 (2014).

Figure 1. Schematic of experimental protocol showing formation of a MNP-labeled cell hydrogel. Hydrogel constructs visualised using z-stack fluorescence microscopy and Magnetic Resonance Imaging.

Nanoparticle-labeled cell hydrogels were formed by (**a**) exogenously labeling cortical astrocytes with MNPs utilising a magnetofection protocol [static magnetic field (F0); 30 mins application]. Labeled cells (**b**) were trypsinized and added to a Collagen I solution, resulting in formation of a MNP-labeled cell hydrogel in a well plate. After 1 h, medium was added over the hydrogel and at 3 h post-construct, the hydrogel was carefully transferred to a larger well to allow it to free-float in medium. Free-floating facilitated homogenous cellular distribution throughout the hydrogel. Following construct, the hydrogels were visualised using (**c**) z-stack fluorescence microscopy and (**d**) MRI. MNP: magnetic nanoparticle; MRI: magnetic resonance imaging

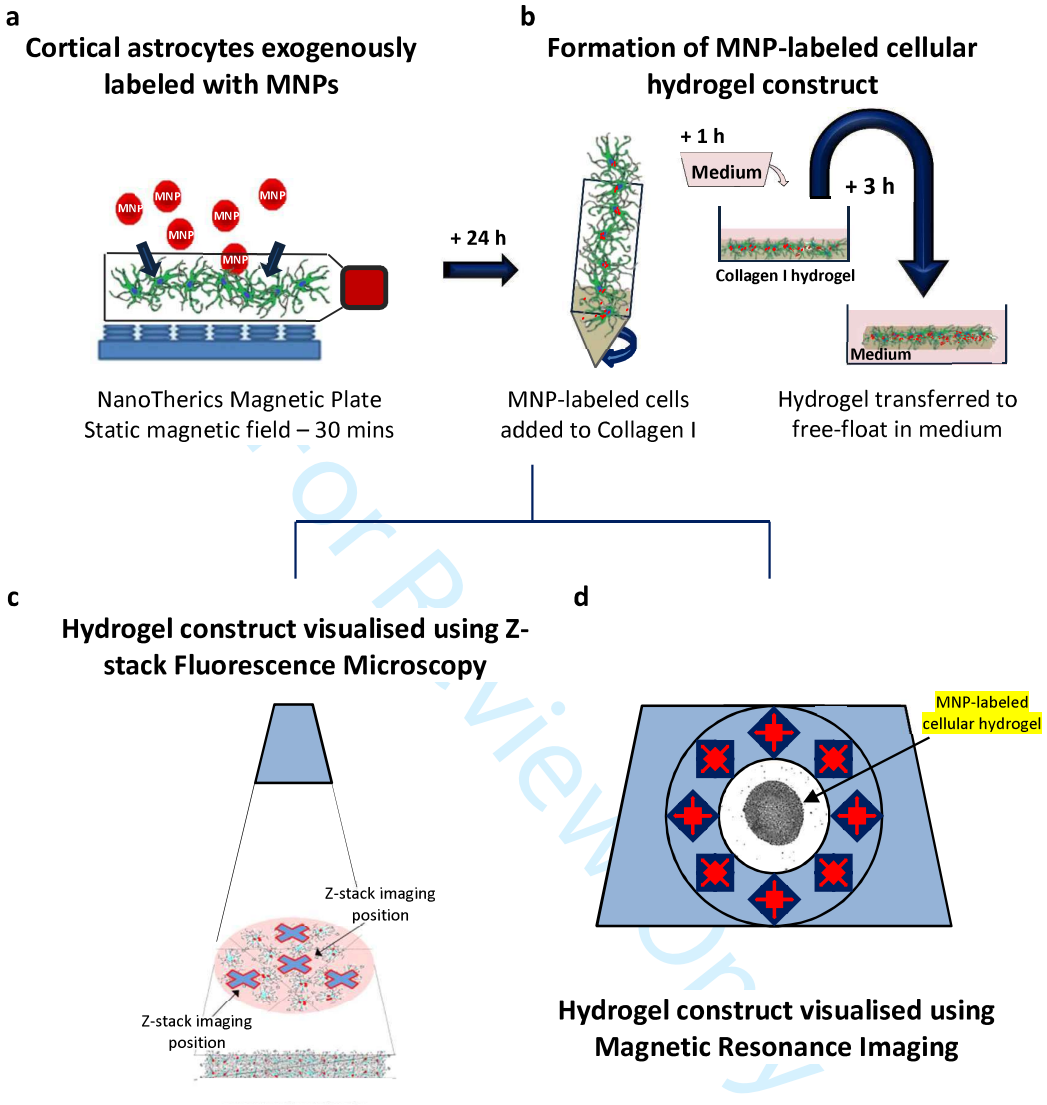

Figure 1. Schematic of experimental protocol showing formation of a MNP-labeled cell hydrogel. Hydrogel constructs visualised using z-stack fluorescence microscopy and Magnetic Resonance Imaging

Figure 2. 3-dimensional cell hydrogels facilitate a complex cellular network of cortical astrocytes

Representative z-stack fluorescence images (**a – c**) showing an emergent complex, connective non MNP-labeled astrocyte network over 14 d. Note the rounded morphology (**a**) at 24 h following addition of cells to the collagen solution. Note the small minority of cells that are beginning to show process elaboration (arrow). At 7 d (**b**), cells show elongated processes and the emergence of a connective network (arrow). At 14 d (**c**), a highly connective, complex cellular network is evident throughout the hydrogel. Bar charts displaying (**d**) average cell count (*p <0.05; 24 h *vs*. 7 d & 14 d) and (**e**) cellular viability (as measured by live/dead assays) of cellular hydrogels over 14 d post-construct. Photographs (**f**) of gel contraction in cellular hydrogels over 14 d post-construct. Graph (**g**) showing hydrogel contraction (diameter) over 14 d. Differences indicated in terms of average cell count *vs.* 24 h; in terms of gel contraction *vs* 0 h (*p <0.05; **p <0.01; ***p <0.001), and *vs* each time point (^p <0.05; ^^p <0.01; ^^^p <0.001) (Cells immunostained for GFAP; FITC secondary antibodies). *Scale = (a - c) 50 μm. n = 3.*

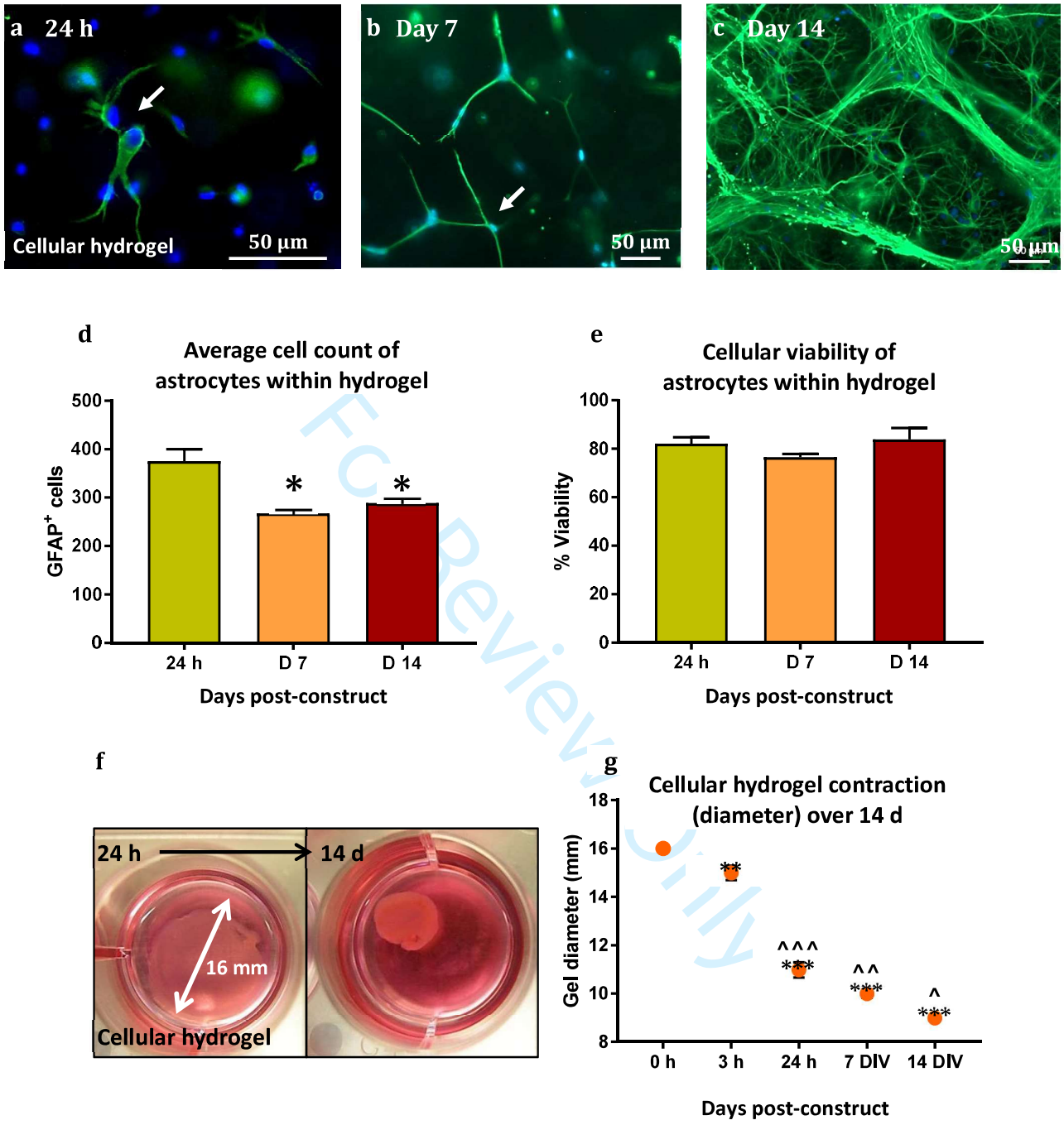

Figure 2. 3-dimensional cell hydrogels facilitate a complex cellular network of cortical astrocytes

Figure 3. Morphological characterisation of unlabeled and MNP-labeled GFAP$^+$ cells in 3-dimensional cell hydrogels

Bar charts displaying the (**a**) rounded/ramified nature of cells; (**b**) average cell area; (**c**) average number of primary processes and (**d**) average length ratio of primary processes of unlabeled and MNP-labeled cell hydrogels over 14 d post-construct (***p <0.001; 24 h *vs*. 14 d).

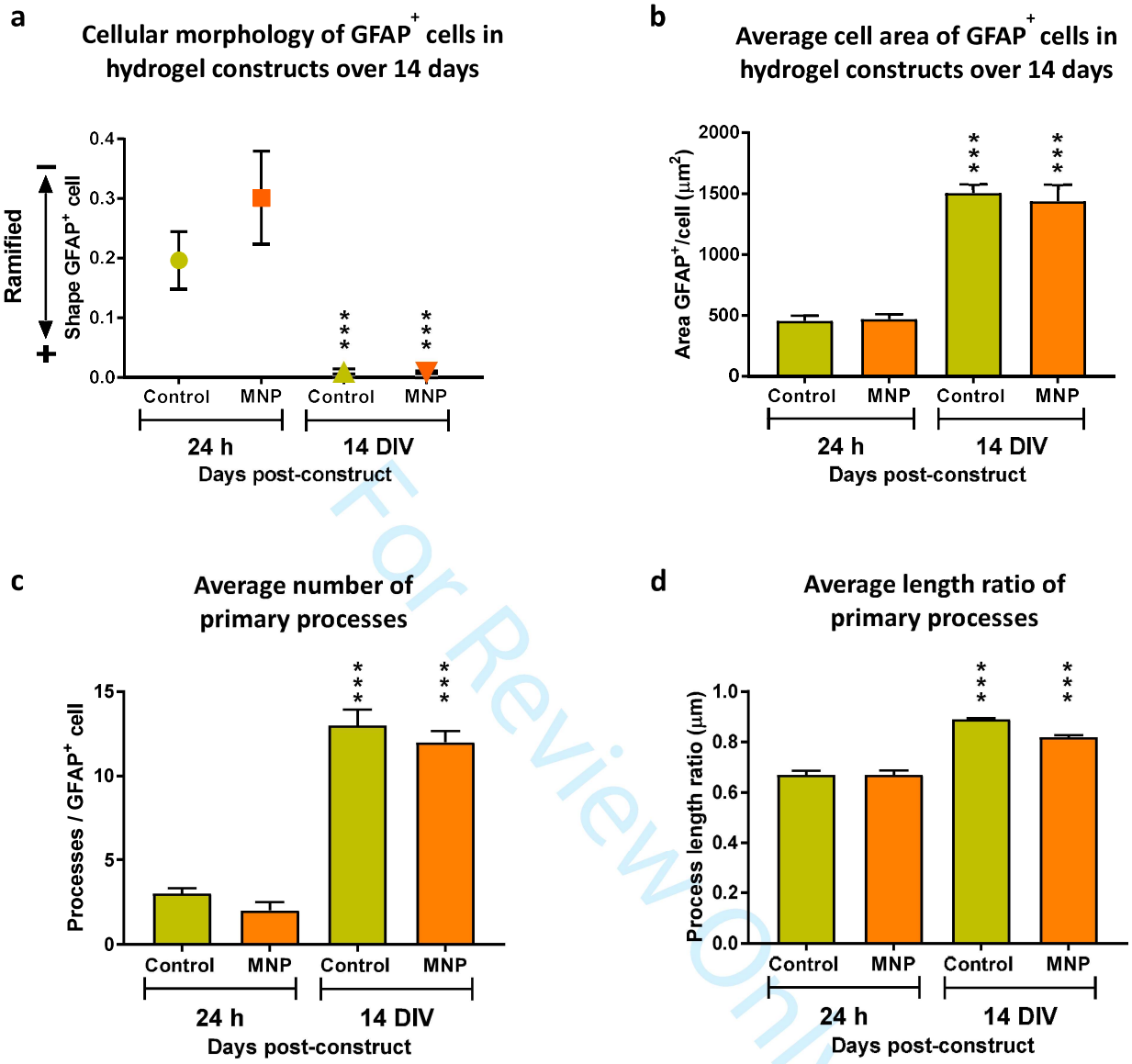

Figure 3. Morphological characterisation of unlabeled and MNP-labeled GFAP$^+$ cells in 3-dimensional cell hydrogels

Figure 4. High magnetite concentration MNPs offer utility for non-invasive tracking of cells over time

Representative fluorescence triple-merged micrograph (**a**) of cortical astrocytes on plastic substrate prior to enzymatic detachment and addition to collagen solution. Z-stack fluorescence image (**b**) of the same cells at 24 h post-hydrogel-construct. Note the difference in cellular morphology. Note the high level of intracellular particle accumulation and co-localisation of particles with cells at this early time point [(**b**) arrows]. Representative orthogonal z-stack fluorescence micrograph (**c**) showing a highly connective, MNP-labeled, cellular network within a MNP-labeled cell hydrogel at 14 d. Representative TEM micrograph (**d**) of a MNP-labeled cell hydrogel at 15 d post-construct. Note the high level of intracellular particle retention and the peri-nuclear localisation of the particles [(**d**) arrows] at this time-point. Note also the collagen fibrils of the hydrogel [(**d**) arrow heads]. Bar charts displaying (**e**) average cell count and (**f**) cellular viability (as measured by live/dead assays) of MNP-labeled cell hydrogels over 14 d post-construct (*p <0.05; 24 h *vs.* 7 d). T_2^*-weighted MR images of (**g**) MNP-labeled and (**h**) unlabeled cell hydrogels at 24 h post-construct, and (**i**) MNP-labeled and (**j**) unlabeled cell hydrogels at 14 d (arrows). Note the hypointense signal recorded from the MNP-labeled cell hydrogels (**g & i**) at both time points, which is not seen in unlabeled cell hydrogels (**h & j**). *[Scale (a - c) 50 µm; (d5 µm; inset 0.25 µm); (g – j) 5 mm] n = 3.* Nu: nucleus; MNP: magnetic nanoparticle; MR: magnetic resonance; TEM: transmission electron microscopy

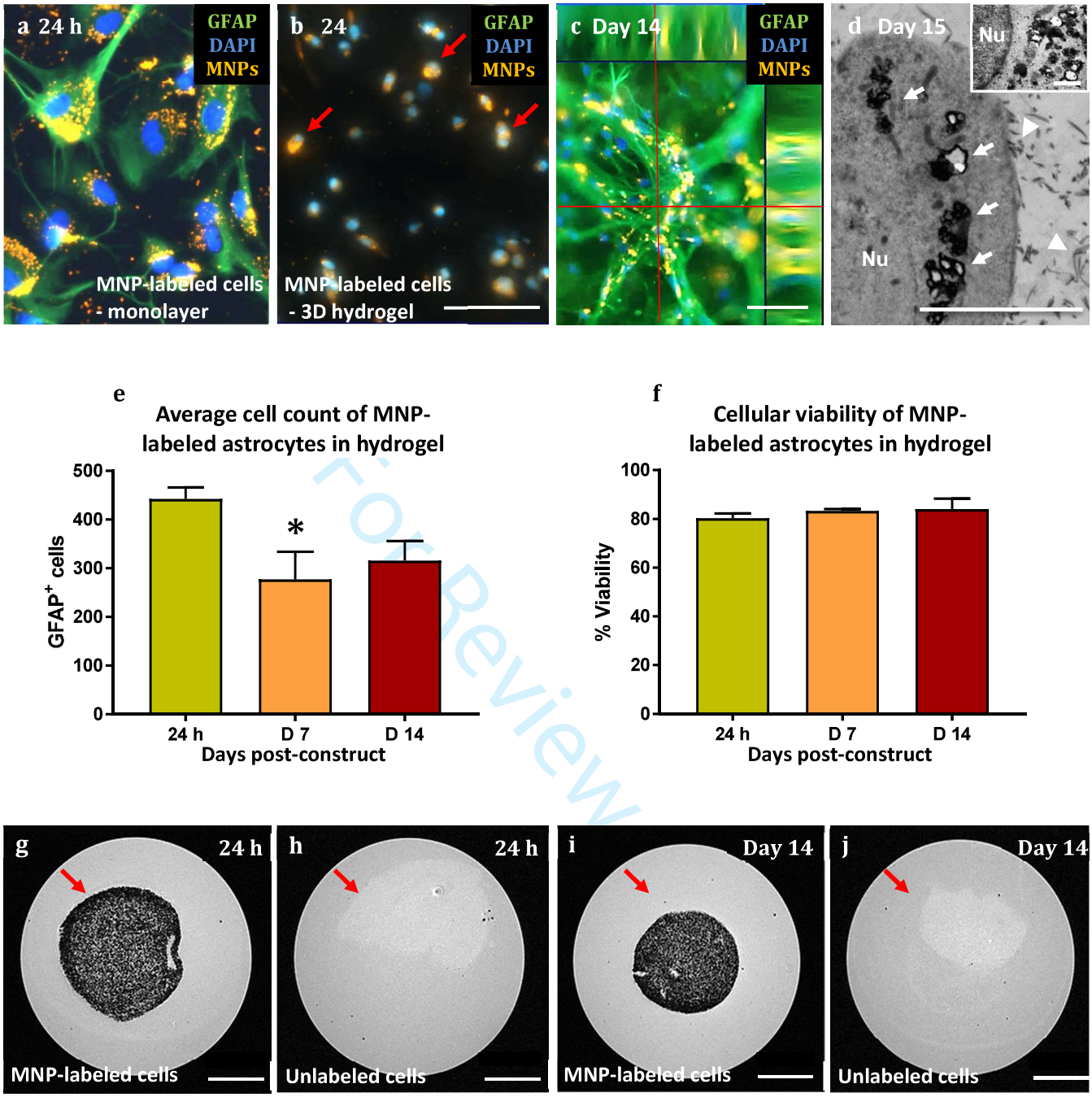

Figure 4. High magnetite concentration MNPs offer utility for non-invasive tracking of cells over time

Figure 5. Unlabeled and MNP-labeled cell hydrogels exhibit a low proliferation profile

Double-merged fluorescence image (**a**) of dividing astrocytes within a cellular hydrogel at 14 d post-construct. Bar graph (**b**) displaying EdU labeling (%) of proliferating cortical astrocytes in unlabeled and MNP-labeled cell hydrogels over 14 d post-construct. Proliferation was significantly higher at 24 h post-construct vs 7 d and 14 d in both unlabeled and MNP-labeled cell hydrogels. Representative sequential still images (**c - h**) taken from dynamic time-lapse imaging (*see Electronic Supplementary Material*) showing a MNP-labeled cortical astrocyte undergoing division at 7 d post-hydrogel-construct. Daughter cells (**h**) exhibit a symmetrical profile of particle inheritance (arrows). (*p <0.05) *(Scale = 50 μm) n = 3.* MNP: magnetic nanoparticle

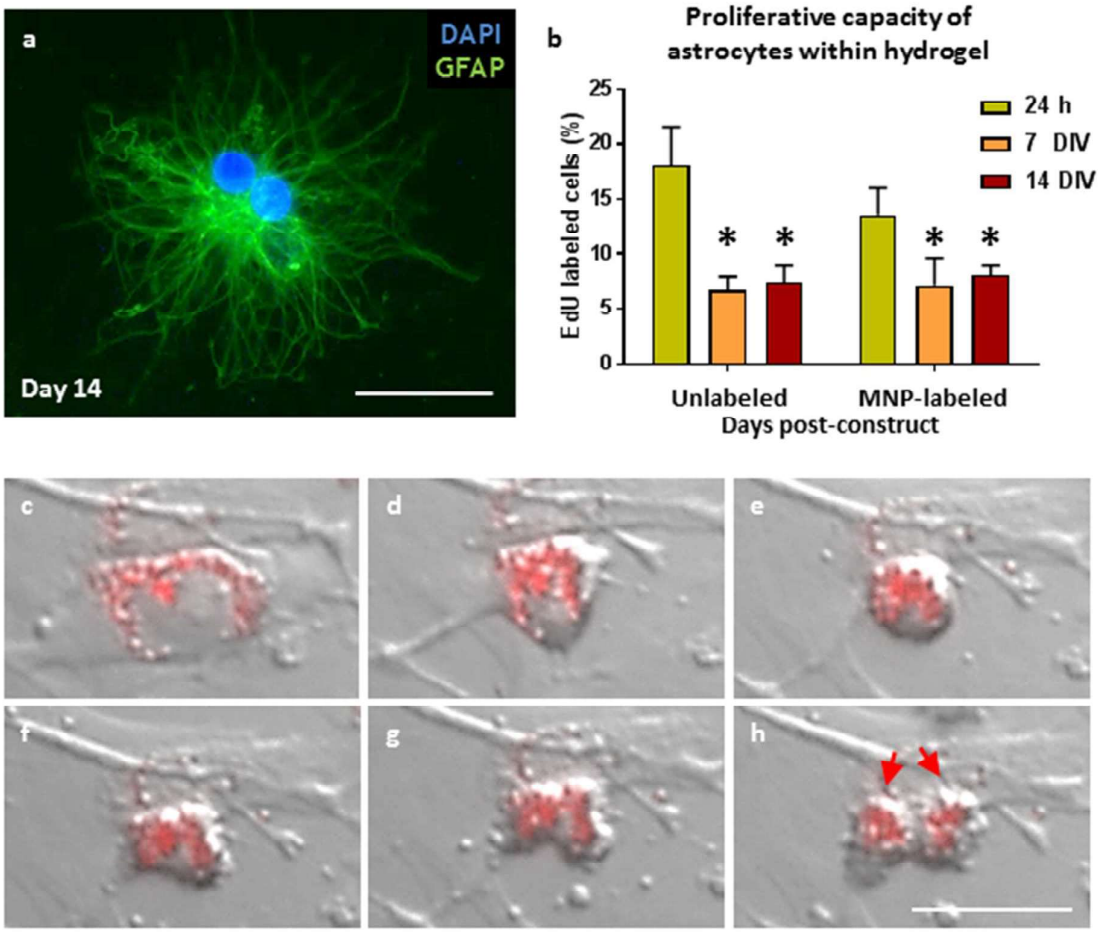

Figure 5. Unlabeled and MNP-labeled cell hydrogels exhibit a low proliferation profile

Figure 6. MRI shows hypointense signal from MNP-labeled cell hydrogels over an extended time period.

MR image (**a**) showing a hypointense signal from the MNP-labeled cell hydrogel at 37 d post-construct, versus (**b**) the hyperintense signal recorded from the unlabeled cell hydrogel at the same time-point (**a & b**; arrows). Confocal fluorescence micrograph (**c**) showing a high level of intracellular particle retention and peri-nuclear localisation of particles at 37 d post-construct [(**c**) arrows]. Representative z-stack fluorescence micrograph (**d**) of a MNP-labeled cell hydrogel at 37 d post-construct *[Scale = (a & b) 5 mm; (c) 100 µm; (d) 50 µm] n = 3.* MNP: magnetic nanoparticle; MRI: magnetic resonance imaging

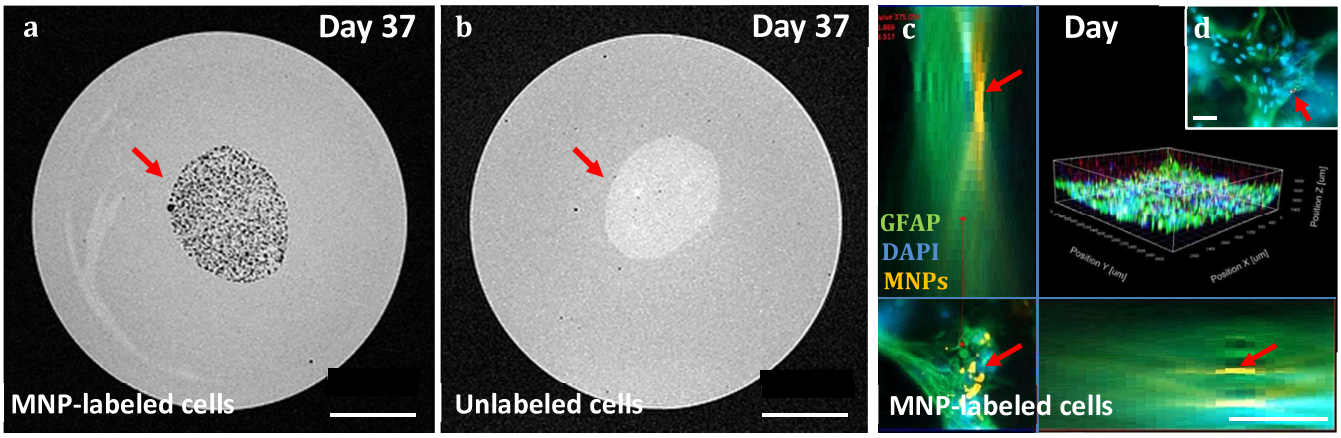

Figure 6. MRI shows hypointense signal from MNP-labeled cell hydrogels over an extended time period.

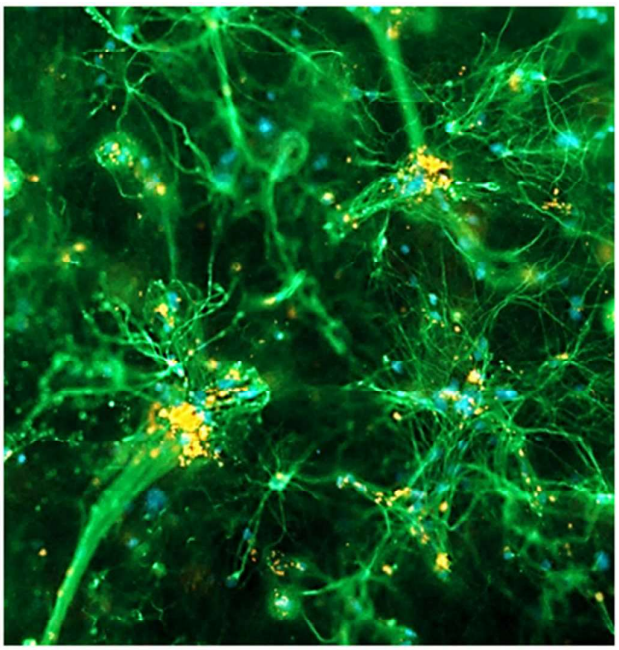

Cover figure (if required) –3-dimensional hydrogels facilitate a complex cellular network of MNP-labeled cortical astrocytes (21 d).